

**REPORT DOCUMENTATION PAGE**Form Approved  
OMB No. 0704-0188

Public reporting burden for this collection of information is estimated to average 1 hour per response, including the time for reviewing instructions, searching existing data sources, gathering and maintaining the data needed, and completing and reviewing this collection of information. Send comments regarding this burden estimate or any other aspect of this collection of information, including suggestions for reducing this burden to Department of Defense, Washington Headquarters Services, Directorate for Information Operations and Reports (0704-0188), 1215 Jefferson Davis Highway, Suite 1204, Arlington, VA 22202-4302. Respondents should be aware that notwithstanding any other provision of law, no person shall be subject to any penalty for failing to comply with a collection of information if it does not display a currently valid OMB control number. **PLEASE DO NOT RETURN YOUR FORM TO THE ABOVE ADDRESS.**

<b>1. REPORT DATE (DD-MM-YYYY)</b> 2002		<b>2. REPORT TYPE</b> Conference paper		<b>3. DATES COVERED (From - To)</b> 2001-2002	
<b>4. TITLE AND SUBTITLE</b> Modeling Relative Position, Relative Velocity, and Range Rate  for Formation Flying				<b>5a. CONTRACT NUMBER</b>	
				<b>5b. GRANT NUMBER</b>	
				<b>5c. PROGRAM ELEMENT NUMBER</b>	
<b>6. AUTHOR(S)</b> Craig A. McLaughlin, Chris Sabol, Aaron Swank, Richard D. Burns, K. Kim Luu				<b>5d. PROJECT NUMBER</b>	
				<b>5e. TASK NUMBER</b>	
				<b>5f. WORK UNIT NUMBER</b>	
<b>7. PERFORMING ORGANIZATION NAME(S) AND ADDRESS(ES)</b> Air Force Research Laboratory Space Vehicles Directorate Directed Energy Directorate 3550 Aberdeen Ave SE Kirtland AFB, NM 87117-5776				<b>8. PERFORMING ORGANIZATION REPORT NUMBER</b>	
<b>9. SPONSORING / MONITORING AGENCY NAME(S) AND ADDRESS(ES)</b>				<b>10. SPONSOR/MONITOR'S ACRONYM(S)</b>	
				<b>11. SPONSOR/MONITOR'S REPORT NUMBER(S)</b>	
<b>12. DISTRIBUTION / AVAILABILITY STATEMENT</b>  Approved for public release; distribution is unlimited.					
<b>13. SUPPLEMENTARY NOTES</b> Published in Advances in the Astronautical Sciences; 2002; v.109 III, p. 2165-2186.					
<b>14. ABSTRACT</b> The relative position, relative velocity, and range rate evolution is examined for various formations of satellites. A simple analytical model including Earth oblateness effects for the equations of relative motion is presented. This model provides physical insight into the Earth oblateness effects that are neglected by using Hill's equations. The accuracy of the relative position, relative velocity, and range rate predictions for the analytical model are compared to realistic force modeling obtained using the Draper Semianalytical Satellite Theory for Formations of varying size, inclination, and altitude.					
<b>15. SUBJECT TERMS</b> Space flight; satellites; Earth (planet); equations of motion; matrix algebra; Earth oblateness effects					
<b>16. SECURITY CLASSIFICATION OF:</b>			<b>17. LIMITATION OF ABSTRACT</b>	<b>18. NUMBER OF PAGES</b>	<b>19a. NAME OF RESPONSIBLE PERSON</b>
<b>a. REPORT</b> Unclassified	<b>b. ABSTRACT</b> Unclassified	<b>c. THIS PAGE</b> Unclassified			Craig A. McLaughlin
			Unlimited	23	<b>19b. TELEPHONE NUMBER (include area code)</b> 505-846-5963

## MODELING RELATIVE POSITION, RELATIVE VELOCITY, AND RANGE RATE FOR FORMATION FLYING

Craig A. McLaughlin,<sup>\*</sup> Chris Sabol,<sup>†</sup> Aaron Swank,<sup>‡</sup>  
Richard D. Burns<sup>\*\*</sup> and K. Kim Luu<sup>††</sup>

The relative position, relative velocity, and range rate evolution is examined for various formations of satellites. A simple analytical model including Earth oblateness effects for the equations of relative motion is presented. This model provides physical insight into the Earth oblateness effects that are neglected by using Hill's equations. The accuracy of the relative position, relative velocity, and range rate predictions for the analytical model are compared to realistic force modeling obtained using the Draper Semianalytical Satellite Theory for formations of varying size, inclination, and altitude.

### INTRODUCTION

Several missions flying satellites in formation are under development or have been recently launched. The relative velocity and range rate have lately become a larger concern for formation flying missions. How and Tillerson<sup>7</sup> show that expected relative velocity measurement errors of 2-3 mm/s have a significant effect on the relative estimation and control problem. This causes an increase in the amount of fuel required to maintain a formation of satellites. One solution to this problem is to provide improved relative navigation measurements through an intersatellite range and range rate sensor. Such a sensor may be subject to constraints on the allowable range and range rate. Most analyses have concentrated on the relative position accuracy. This paper presents an analysis of relative position, relative velocity, and range rate. In addition, a simple analytical model is developed that provides physical insight into Earth oblateness effects that are ignored when using Hill's equations. This model was developed to address the need for a way to describe the relative position, velocity, and range rate of the satellites in a formation that attained a high level of accuracy, but was easy to use and understand. In addition, the model provides physical insight into the effects of  $J_2$  on the relative equations of motion using classical descriptions of orbital mechanics.

Sabol et al.<sup>12</sup> presented a numerical analysis of satellite formation flying that showed the absolute and relative effects of  $J_2$  are significant for formations of satellites with out-of-plane motion.

\* Air Force Research Laboratory, Space Vehicles Directorate, 3550 Aberdeen Avenue, S.E., Kirkland, AFB, New Mexico 87117-5776. Member AAS; Senior Member AIAA.

† Air Force Research Laboratory, Directed Energy Directorate, 3550 Aberdeen Avenue, S.E., Kirkland, AFB, New Mexico 87117. Member AIAA.

‡ Air Force Research Laboratory, Space Vehicles Directorate, 3550 Aberdeen Avenue, S.E., Kirkland, AFB, New Mexico 87117-5776. Member AIAA.

\*\* Air Force Research Laboratory, Space Vehicles Directorate, 3550 Aberdeen Avenue, S.E., Kirkland, AFB, New Mexico 87117-5776. Member AAS; Member AIAA.

†† Air Force Research Laboratory, Directed Energy Directorate, 3550 Aberdeen Avenue, S.E., Kirkland, AFB, New Mexico 87117. Member AAS.

In addition, they presented a simple analytical description of the reason for the observed motion in terms of  $J_2$ . However, that analysis only looked at polar orbits. Alfriend et al.<sup>1</sup> developed a state transition matrix to analyze the errors in using Hill's equations for differences in orbital elements. Gim and Alfriend<sup>5</sup> develop this analysis further to produce a state transition matrix of the relative motion including eccentric reference orbits and the effects of  $J_2$ . Inalhan and How<sup>8</sup> present an analysis using a closed form solution for relative motion in eccentric orbits as a function of true anomaly. They rely on a development originally attributed to Lawden.<sup>9</sup>

This paper presents an analysis of the relative position, relative velocity, and range rate of satellites in low eccentricity orbits. If  $x$ ,  $y$ , and  $z$  represent the distance between satellites in the radial, along-track, and cross-track directions and  $\dot{x}$ ,  $\dot{y}$ , and  $\dot{z}$  represent the components of relative velocity in those directions then the range  $\rho$ , relative velocity  $v$ , and the range rate  $\dot{\rho}$  are

$$\begin{aligned} (1) \quad & \rho^2 = x^2 + y^2 + z^2 \\ (2) \quad & v^2 = \dot{x}^2 + \dot{y}^2 + \dot{z}^2 \\ (3) \quad & \dot{\rho} = (x\dot{x} + y\dot{y} + z\dot{z})/\rho \end{aligned}$$

These equations hold regardless of the method used to calculate the relative positions and velocities.

In general the differential equations describing the relative motion of satellites where the reference satellite is in a near circular orbit and the relative separation is small compared to the radius of the orbit are

$$\begin{aligned} (4) \quad & \ddot{x} - 2w_{xy}\dot{y} - 3w_z^2x = f_x \\ (5) \quad & \ddot{y} + 2w_{xy}\dot{x} = f_y \\ (6) \quad & \ddot{z} + w_z^2z = f_z \end{aligned}$$

where  $w_{xy}$  is the frequency of the in-plane motion,  $w_z$  is the frequency of the out-of-plane motion, and  $f_x$ ,  $f_y$ , and  $f_z$  represent the relative perturbing forces. For a spherical Earth as in Hill's equations,  $w_{xy} = w_z = n$ , where  $n$  is the mean motion.

The Draper Semianalytical Satellite Theory was used to model the truth of the mean element evolution of the satellite formations using realistic dynamics. An analytical model was developed that accurately captures the effects of  $J_2$  on the formation evolution. Results of the model were compared to DSST for formations with a variety of inclinations. In addition, the effects of altitude and formation size are examined.

## Hill's Equations

Hill's equations<sup>6</sup> are commonly used for formation design and analysis. Sabol et al.,<sup>12</sup> Alfriend et al.,<sup>1</sup> and Inalhan and How<sup>8</sup> point out some of the limitations of using Hill's equations. These limitations arise from assuming the reference orbit is circular and the Earth is a perfect sphere.

Vallado<sup>16</sup> provides a detailed derivation of Hill's equations and the solution for unperturbed motion for both relative position and velocity. The solutions for unperturbed motion are

$$\begin{aligned} (7) \quad & x = (\dot{x}_0/n) \sin nt - [3x_0 + (2\dot{y}_0/n)] \cos nt + 4x_0 + 2\dot{y}_0/n \\ (8) \quad & y = (2\dot{x}_0/n) \cos nt + [6x_0 + (4\dot{y}_0/n)] \sin nt - (6nx_0 + 3\dot{y}_0)t - 2\dot{x}_0/n + y_0 \\ (9) \quad & z = (\dot{z}_0/n) \sin nt + z_0 \cos nt \\ (10) \quad & \dot{x} = \dot{x}_0 \cos nt + (3nx_0 + 2\dot{y}_0) \sin nt \\ (11) \quad & \dot{y} = -2\dot{x}_0 \sin nt + (6nx_0 + 4\dot{y}_0) \cos nt - (6nx_0 + 3\dot{y}_0) \\ (12) \quad & \dot{z} = \dot{z}_0 \cos nt - nz_0 \sin nt \end{aligned}$$

Table 1: Initial conditions for circular and projected circular formations

Formation	$x_0$	$\dot{x}_0$	$y_0$	$\dot{y}_0$	$z_0$	$\dot{z}_0$
Circular	$(\rho_0/2) \cos \theta$	$-(\rho_0 n/2) \sin \theta$	$2\dot{x}_0/n$	$-2n\dot{x}_0$	$\pm\sqrt{3}x_0$	$\pm\sqrt{3}\dot{x}_0$
Projected Circular	$(\rho'_0/2) \cos \theta$	$-(\rho'_0 n/2) \sin \theta$	$2\dot{x}_0/n$	$-2n\dot{x}_0$	$\pm 2x_0$	$\pm 2\dot{x}_0$

where the subscript 0 values are initial conditions. Vallado<sup>16</sup> and Sabol et al.<sup>12</sup> provide more detailed analyses of the motion that results from Hill's equations. Of particular interest for this study are the circular and projected circular formations presented in Sabol et al.<sup>12</sup> The circular formation has relative motion in a circle about the reference trajectory. The projected circular formation projects a circle on the  $yz$ -plane and thus onto the Earth below. The initial conditions for these formations are given in Table 1.  $\rho_0$  is the radius of the circle,  $\rho'_0$  is the radius of the projected circle, and  $\theta$  is the phase angle in the circle or projected circle measured counterclockwise from the  $z$  axis. The  $y_0$  and  $\dot{y}_0$  conditions set the along-track offset and drift to zero. The signs on the  $z_0$  and  $\dot{z}_0$  conditions must be the same. There are two planes in which both the circular and projected circular formation are possible. Both intersect the cross-track/along-track plane along the along-track axis. The circular formation is inclined to that plane at  $\pm 30^\circ$ . The projected circular is inclined at  $\pm 26.565^\circ$  to that plane.

## RELATIVE MOTION INCLUDING $J_2$

The primary perturbation affecting formation flying satellites of identical area-to-mass ratio is Earth oblateness. This is represented by the factor  $J_2$ . The first order secular effects of  $J_2$  on the right ascension of the ascending node  $\Omega$ , the argument of perigee  $\omega$ , and the mean anomaly  $M$  are given by

$$(13) \quad \dot{\Omega} = -\frac{3nR_E^2 J_2}{2p^2} \cos i$$

$$(14) \quad \dot{\omega} = \frac{3nR_E^2 J_2}{4p^2} (4 - 5 \sin^2 i)$$

$$(15) \quad \dot{M} = \frac{3nR_E^2 J_2 \sqrt{1 - e^2}}{4p^2} (2 - 3 \sin^2 i)$$

where  $R_E$  is the equatorial radius of Earth,  $e$  is the eccentricity,  $p$  is the semilatus rectum, and  $i$  is the inclination. As reported in Sabol et al.<sup>12</sup> the  $J_2$  perturbations have two primary effects on satellites flying in formation. The first is a long periodic effect because the in-plane ( $xy$ ) motion has a period that depends on perigee passing, but the out-of-plane ( $z$ ) motion has a period that depends on nodal crossing. The second effect applies to satellites with inclination differences. In this case the above equations show that there are differential perturbations which cause secular growth in the separation of the satellites. The remainder of this section develops successively more complex equations to describe the relative motion of satellites affected by  $J_2$ . The limitations that the satellites are in near circular orbits and that the relative separation between the satellites is small relative to the orbit radii will still apply to these equations.

### Satellites With Matching Inclinations

Differences in either right ascension of the ascending node  $\Omega$  or inclination  $i$  provide out-of-plane ( $z$ ) motion described in Hill's equations. In both cases the following effects will be present.

According to Hill's equations all three components have motion with a frequency governed by the mean motion  $n$ . However, the frequency of the  $x$  and  $y$  components are actually determined by the satellites passing perigee. For orbits perturbed by  $J_2$  this is governed by  $(n + \dot{M})$ . The frequency of the  $z$  component is actually determined by nodal crossing time. This frequency is governed by  $(n + \dot{M} + \dot{\omega})$  for orbits perturbed by  $J_2$ . The resulting motion is described by

$$(16) \quad x = (\dot{x}_0/w_{xy}) \sin w_{xy}t - (3x_0 + 2\dot{y}_0/w_{xy}) \cos w_{xy}t + 4x_0 + 2\dot{y}_0/w_{xy}$$

$$(17) \quad y = (6x_0 + 4\dot{y}_0/w_{xy}) \sin w_{xy}t + (2\dot{x}_0/w_{xy}) \cos w_{xy}t - (6w_{xy}x_0 + 3\dot{y}_0)t + y_0 - 2\dot{x}_0/w_{xy}$$

$$(18) \quad z = z_0 \cos w_z t + (\dot{z}_0/w_z) \sin w_z t$$

$$(19) \quad \dot{x} = \dot{x}_0 \cos w_{xy}t + (3w_{xy}x_0 + 2\dot{y}_0) \sin w_{xy}t$$

$$(20) \quad \dot{y} = (6w_{xy}x_0 + 4\dot{y}_0) \cos w_{xy}t - 2\dot{x}_0 \sin w_{xy}t - (6w_{xy}x_0 + 3\dot{y}_0)$$

$$(21) \quad \dot{z} = -w_z z_0 \sin w_z t + \dot{z}_0 \cos w_z t$$

where

$$(22) \quad w_{xy} = n + \dot{M}$$

$$(23) \quad w_z = n + \dot{M} + \dot{\omega}$$

These are the same as the solutions to Hill's equations except that  $w_{xy}$  replaces  $n$  in the  $x$  and  $y$  terms, and  $w_z$  replaces  $n$  in the  $z$  term. The relative velocities are simply the time derivatives of the relative positions. The initial conditions in Hill's equations were used to determine the initial mean orbital elements in DSST. However, the initial conditions in the model are calculated using  $w_{xy}$  and  $w_z$  instead of  $n$  as in Table 1. The relative separation in each component will not grow with time, but the phasing of the motion will cause the overall separation to have a long period effect. These equations predict that there will be no separation growth at critical inclination. For satellites that have  $z$  motion caused only by differences in  $\Omega$  these equations accurately describe the relative motion in all three components.

## Satellites With Inclination Differences

Differential effects on  $\Omega$ ,  $\omega$ , and  $M$  occur when the satellites have different inclinations. In this case  $J_2$  affects both the  $y$  and  $z$  motion. In the  $z$  equation an additional term appears containing  $\delta\dot{\Omega}t$ . This term, which represents the effect of the differential precession of  $\Omega$ , will slowly grow with time. However, the  $y$  equation has an additional term that contains all the differential rates ( $\delta\dot{\Omega}$ ,  $\delta\dot{\omega}$ , and  $\delta\dot{M}$ ) multiplied by time. The  $\delta\dot{\Omega}$  part of the term represents the differential precession of  $\Omega$ . The rest of the term represents the along-track effects of differential rates of  $\dot{\omega}$  and  $\dot{M}$ . This term may grow quickly with time depending on the inclination. The final set of equations is now

$$(24) \quad x = (\dot{x}_0/w_{xy}) \sin w_{xy}t - (3x_0 + 2\dot{y}_0/w_{xy}) \cos w_{xy}t + 4x_0 + 2\dot{y}_0/w_{xy}$$

$$(25) \quad y = (6x_0 + 4\dot{y}_0/w_{xy}) \sin w_{xy}t + (2\dot{x}_0/w_{xy}) \cos w_{xy}t - (6w_{xy}x_0 + 3\dot{y}_0)t + y_0 - 2\dot{x}_0/w_{xy} \\ + a(\delta\dot{\Omega} \cos i + \delta\dot{\omega} + \delta\dot{M})t$$

$$(26) \quad z = z_0 \cos w_z t + (\dot{z}_0/w_z) \sin w_z t - a\delta\dot{\Omega}t \sin i \cos w_z t$$

$$(27) \quad \dot{x} = \dot{x}_0 \cos w_{xy}t + (3w_{xy}x_0 + 2\dot{y}_0) \sin w_{xy}t$$

$$(28) \quad \dot{y} = (6w_{xy}x_0 + 4\dot{y}_0) \cos w_{xy}t - 2\dot{x}_0 \sin w_{xy}t - (6w_{xy}x_0 + 3\dot{y}_0) + a(\delta\dot{\Omega} \cos i + \delta\dot{\omega} + \delta\dot{M})$$

$$(29) \quad \dot{z} = -w_z z_0 \sin w_z t + \dot{z}_0 \cos w_z t - a\delta\dot{\Omega} \sin i [\cos w_z t - tw_z \sin w_z t]$$

Because of the perturbation terms the initial conditions on the velocity will have a bias compared to DSST in the  $y$  and  $z$  terms for satellites that have inclination differences. This will be apparent in the results presented later.

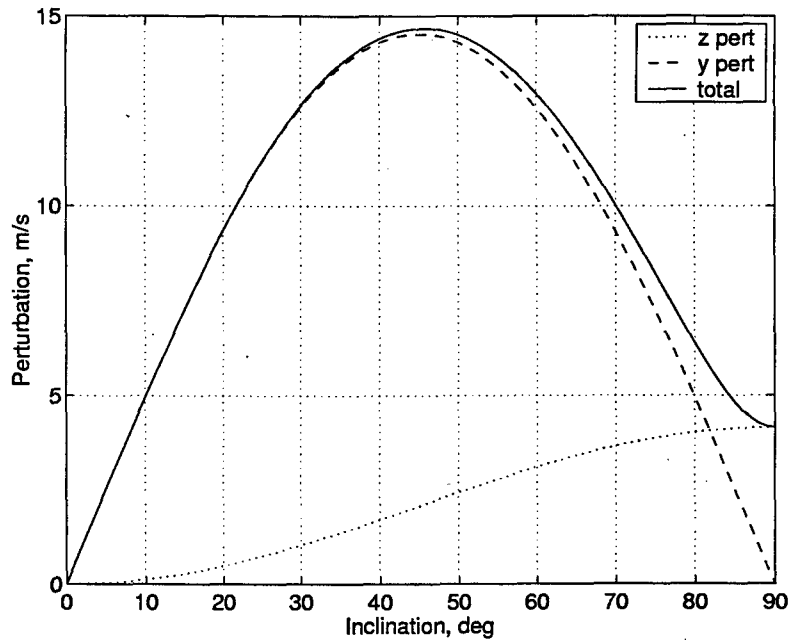


Figure 1: Perturbations caused by  $J_2$  as a function of inclination for an 800 km altitude, 1 km radius circular formation

If  $e^2$  terms are ignored and  $k = 3nR_E^2 J_2 / 2p^2$  the differential rates caused by  $J_2$  of  $\dot{\Omega}$ ,  $\dot{\omega}$ , and  $\dot{M}$  are

$$(30) \quad \delta\dot{\Omega} = k \sin i \delta i$$

$$(31) \quad \delta\dot{\omega} = -5k \sin i \cos i \delta i$$

$$(32) \quad \delta\dot{M} = -3k \sin i \cos i \delta i$$

The secular term caused by  $J_2$  in the  $y$  equation then becomes

$$(33) \quad a(\delta\dot{\Omega} \cos i + \delta\dot{\omega} + \delta\dot{M})t = -7atk \sin i \cos i \delta i$$

This equation shows that the secular term in  $y$  is zero for inclinations of  $0^\circ$ ,  $90^\circ$ , and  $180^\circ$ . The maximum growth will occur at inclinations of  $45^\circ$  and  $135^\circ$ . The new term in the  $z$  equation is periodic with a secularly increasing amplitude. Substituting in this term yields

$$(34) \quad -a\delta\dot{\Omega}t \sin i \cos w_z t = -at \cos w_z t k \sin^2 i \delta i$$

This equation shows the term will be maximum for a polar orbit and zero for an equatorial orbit. The differential  $J_2$  terms used in the results section were found by differencing the actual rates from Eqs. 13 through 15 for each orbit instead of using Eqs. 30 through 32. Fig. 1 shows the relative velocity magnitude added by the  $J_2$  perturbation to the  $y$ ,  $z$ , and total relative motion as a function of inclination. The figure shows that except for high inclinations the  $y$  perturbation is the dominant perturbation. Also, the maximum perturbation occurs at an inclination of just over  $45^\circ$ . However, the  $z$  perturbation is out-of-plane and, therefore, will probably be more expensive to correct than the  $y$  perturbation.

## PROPAGATIONS

Test cases for each of the four formation designs were propagated for four days in the presence of realistic dynamics. The DSST Averaged Orbit Generator (AOG) was used to propagate mean elements for each of the test cases. DSST was chosen for its rigorous modeling of the averaged equations of motion. This allows for fast, efficient, and accurate orbit propagation over long periods using step sizes on the order of one day. McClain,<sup>10</sup> Danielson,<sup>2</sup> Feiger,<sup>3</sup> Sabol et al.,<sup>13</sup> and Fonte<sup>4</sup> provide more information on the formulation and accuracy of the DSST. The DSST runs were executed with the Draper Research and Development version of the Goddard Trajectory Determination System (DGTDS).<sup>4</sup> The mean elements were propagated because the mean evolution of the motion is what is important for comparing the satellites in a formation. Trying to control the periodic changes in the relative motion caused by periodic changes in the osculating orbital elements would not be advisable unless the satellites are extremely close and there is a risk of collision. However, Proulx et al.<sup>11</sup> provide an examination of the short-periodic effects on formation flying of satellites with different area-to-mass ratios.

The perturbations modeled in the propagations include a geopotential to degree and order 21, atmospheric drag effects, luni-solar third-body point-mass effects, and solar radiation pressure. Table 2 lists the specifics of the ephemeris generations.

Table 2: DSST propagation description

Characteristic	Setting
Start time	Sept. 15, 1998, 0 hr, 0 min, 0 sec
End time	Sept. 19, 1998, 0 hr, 0 min, 0 sec
Integrator	12th-order summed Cowell/Adams predict partial correct
Step size	12 hrs
Geopotential	21x21 JGM2
Atmospheric drag	Jacchia-Roberts, $C_D=2.0$
Third-body	"Hot" Schatten Solar Flux, $k_p$ prediction
Solar radiation pressure	Solar/lunar point masses based on JPL DE ephemerides Cylindrical shadow model, $C_r=1.2$

The Jacchia-Roberts atmospheric density model is dependent upon daily F10.7 cm solar flux and 3-hourly values of the  $k_p$  geomagnetic indices. Schatten<sup>14,15</sup> developed a method to predict smoothed estimates of these parameters over the solar cycle. The solar flux and geomagnetic indices used in this analysis are the "hot" or maximum value predictions from 1994. The "hot" atmosphere prediction provides a conservative estimate of drag effects. Identical area-to-mass ratios of  $0.01 \text{ m}^2/\text{kg}$  were used for each spacecraft in drag and solar radiation pressure calculations.

For each of the formation flying designs, three orbits were propagated: one representing the reference satellite, and the other two representing other satellites in the formation. The trajectories were then compared over four days to examine the relative motion of the formations in the presence of perturbations. The output of the relative velocities from DGTDS ( $\dot{x}_{GTDS}$ ,  $\dot{y}_{GTDS}$ ,  $\dot{z}_{GTDS}$ ) was simply the difference between the relative velocity components of the satellites in an inertial frame. Consequently, the relative velocities had to be adjusted into Hill's frame by subtracting out the  $\dot{\omega}x\hat{r}$  term. The rotation rate is the mean motion  $n$  about the  $z$  axis. Therefore, the relative velocities were adjusted by

$$(35) \quad \dot{x}_{Hill} = \dot{x}_{DGTDS} + n\mathbf{y}$$

$$(36) \quad \dot{y}_{Hil} = \dot{y}_{DGTDS} - nx$$

$$(37) \quad \dot{z}_{Hil} = \dot{z}_{DGTDS}$$

The elements resulting from the formation designs and input into the DGTDS DSST propagator are assumed to be averaged or mean elements. If the Keplerian elements are assumed to be osculating in the presence of perturbations, the mean semimajor axes will not match, and the formation design specifications will not hold.

The basic formations studied were at 800 km altitude with a circle or projected circle with a radius of 1 km. The satellites were assumed to be initially at the ascending node. In all cases satellite 1 is at the origin of the Hill's frame, satellite 2 is at  $\theta = 270^\circ$ , and satellite 3 is at  $\theta = 90^\circ$ . This means that satellite 2 has out-of-plane motion primarily caused by inclination differences and satellite 3 has out-of-plane motion primarily caused by differences in right ascension. The basic formations were examined at reference inclinations of  $1^\circ$ ,  $28.5^\circ$ ,  $45^\circ$ ,  $63.435^\circ$ , and  $90^\circ$ . Each satellite had semimajor axis  $a$  of 7178.1363 km. For all formations satellite 1 always had eccentricity of  $1 \times 10^{-8}$ , reference inclination, and zero right ascension  $\Omega$ , argument of perigee  $\omega$ , and mean anomaly  $M$ . For all of the basic formations satellite 2 always had eccentricity of  $6.965597 \times 10^{-5}$ , and satellite 3 always had eccentricity of  $6.965463 \times 10^{-5}$  for the circular formations and  $6.965705 \times 10^{-5}$  for the projected circular formations. The other initial mean orbital elements for satellites 2 and 3 are given in Table 3.

In addition to the basic 800 km altitude, 1 km circular and projected circular formations, three additional cases were examined. The first was a 1 km projected circular formation at 600 km altitude ( $a = 6978.1363$ ) and  $28.5^\circ$  inclination. The other two were projected circular formations at 800 km altitude and  $28.5^\circ$  inclination. One projected circle had a radius of 10 km and the other had a radius of 100 m. All satellites in a given formation had matching mean semimajor axes. The initial orbital elements of satellites 2 and 3 for the other formations are given in Table 4.

## RESULTS

The results presented are for circular formations with radii of 1 km at 800 km altitude unless specifically stated otherwise. Satellites 1 and 3 have out-of-plane relative motion primarily because of differences in right ascension. Satellites 1 and 2 have out-of-plane relative motion primarily because of differences in inclination.

### Satellites 1 and 3

Since satellites 1 and 3 have little or no inclination differences compared to satellites 1 and 2, it is illustrative to examine these first starting with a polar reference orbit. Figs. 2 through 5 show the results for the relative separations. Each figure shows the evolution obtained from DSST, the  $J_2$  model, and the error of the  $J_2$  model compared to DSST. Although the total separation grows, the separation in each component has only periodic changes and no secular growth. The errors of the  $J_2$  model in the radial component are less than a meter, and the errors in the cross-track component are a few meters. By far the largest error is in the along-track component. The errors shown here are typical of all the cases run.

Figs. 6 through 9 show the results for the relative velocities. Again, each figure shows the evolution obtained from DSST, the  $J_2$  model, and the error of the  $J_2$  model compared to DSST.

Table 3: Initial mean orbital elements for satellites 2 and 3 (Basic formations)

Formation	$i$ , deg	$\Omega$ , deg	$\omega$ , deg	$M$ , deg
<u>Circ.</u>				
<u><math>i = 1^\circ</math></u>				
Sat 2	1.00691260	$5.480 \times 10^{-5}$	270.02478675	89.97515845
Sat 3	1.00002389	0.39610432	359.60395601	0
<u><math>i = 28.5^\circ</math></u>				
Sat 2	28.50691260	$2.09 \times 10^{-6}$	270.02483977	89.97515845
Sat 3	28.50000077	0.01448802	359.98726768	0
<u><math>i = 45^\circ</math></u>				
Sat 2	45.00691260	$1.48 \times 10^{-6}$	270.02484058	89.97515845
Sat 3	45.00000042	$9.77658 \times 10^{-3}$	359.99308692	$1.21 \times 10^{-6}$
<u><math>i = 63.435^\circ</math></u>				
Sat 2	63.44191260	$1.21 \times 10^{-6}$	270.02484106	89.97515845
Sat 3	63.43500021	$7.72906 \times 10^{-3}$	359.99654347	0
<u><math>i = 90^\circ</math></u>				
Sat 2	90.00691260	$1.21 \times 10^{-6}$	270.02484155	89.97515845
Sat 3	90	$6.91308 \times 10^{-3}$	0	$1.21 \times 10^{-6}$
<u>Proj. Circ.</u>				
<u><math>i = 1^\circ</math></u>				
Sat 2	1.00798199	$6.321 \times 10^{-5}$	270.02478675	89.97116746
Sat 3	1.00003186	0.45737944	359.54269022	$1.21 \times 10^{-6}$
<u><math>i = 28.5^\circ</math></u>				
Sat 2	28.50798199	$2.41 \times 10^{-6}$	270.02883049	89.97116746
Sat 3	28.50000102	0.01672932	359.98529799	0
<u><math>i = 45^\circ</math></u>				
Sat 2	45.00798199	$1.71 \times 10^{-6}$	270.02883143	89.97116746
Sat 3	45.00000056	0.01128902	359.99201746	359.99999879
<u><math>i = 63.435^\circ</math></u>				
Sat 2	63.44298199	$1.21 \times 10^{-6}$	270.02883198	89.97116746
Sat 3	63.43500028	$8.92475 \times 10^{-3}$	359.99600874	0
<u><math>i = 90^\circ</math></u>				
Sat 2	90.00798199	$1.21 \times 10^{-6}$	270.02883254	89.97116746
Sat 3	90	$7.98254 \times 10^{-3}$	0	0

Table 4: Initial mean orbital elements for satellites 2 and 3 (Other formations)

Formation	$e$	$i$ , deg	$\Omega$ , deg	$\omega$ , deg	$M$ , deg
<u>Proj. Circ.</u>					
<u><math>i = 28.5^\circ</math></u>					
Alt.=600 km					
Sat 2	$7.165237 \times 10^{-5}$	28.50821076	$2.56 \times 10^{-6}$	270.02983170	89.97016613
Sat 3	$7.165374 \times 10^{-5}$	28.50000108	0.01720883	359.98487658	0
$\rho'_0 = 10$ km					
Sat 2	$6.9656638 \times 10^{-4}$	28.57981973	$2.3245 \times 10^{-4}$	270.31876420	89.68103165
Sat 3	$6.9704276 \times 10^{-4}$	28.50010254	0.16739767	359.85288811	0
$\rho'_0 = 100$ m					
Sat 2	$6.96560 \times 10^{-6}$	28.50079820	0	269.97223875	90.02776123
Sat 3	$6.96188 \times 10^{-6}$	28.50000001	$1.67283 \times 10^{-3}$	359.99852989	0

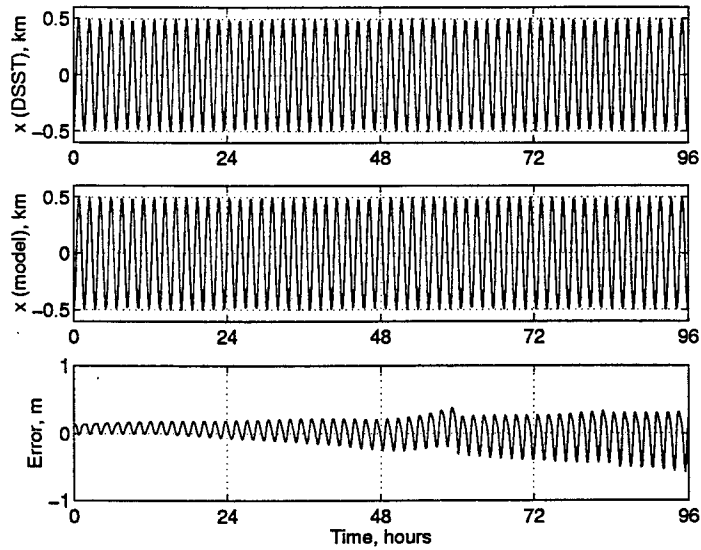


Figure 2: Comparison of the radial separation ( $x$ ) of satellite 1 and 3 from DSST and  $J_2$  model for a 800 km, polar reference orbit. The satellites are in a 1 km circular formation.

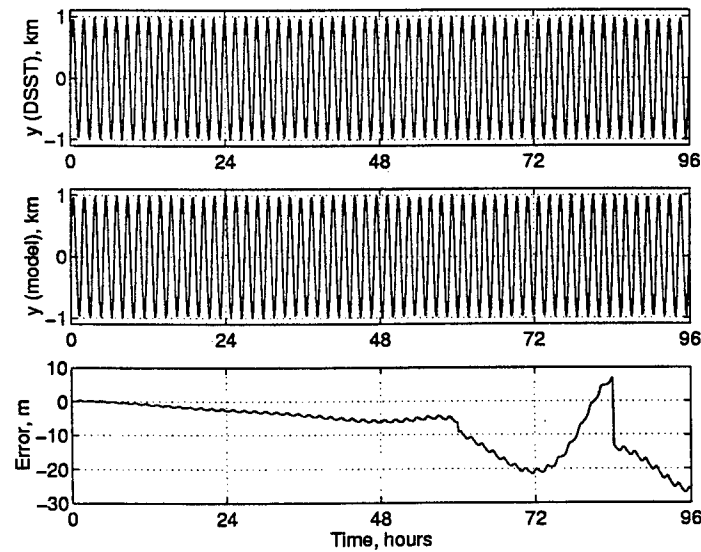


Figure 3: Comparison of the along-track separation ( $y$ ) of satellites 1 and 3 from DSST and  $J_2$  model for a 800 km, polar reference orbit. The satellites are in a 1 km circular formation.

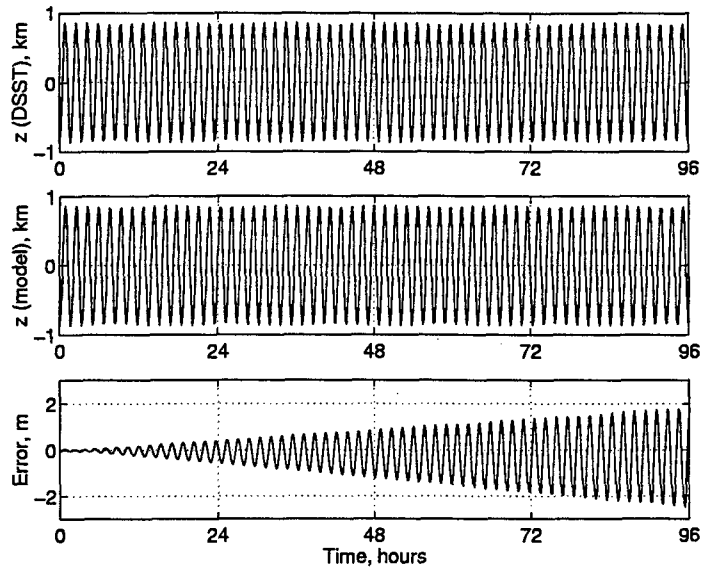


Figure 4: Comparison of the cross-track separation ( $z$ ) of satellites 1 and 3 from DSST and  $J_2$  model for a 800 km, polar reference orbit. The satellites are in a 1 km circular formation.

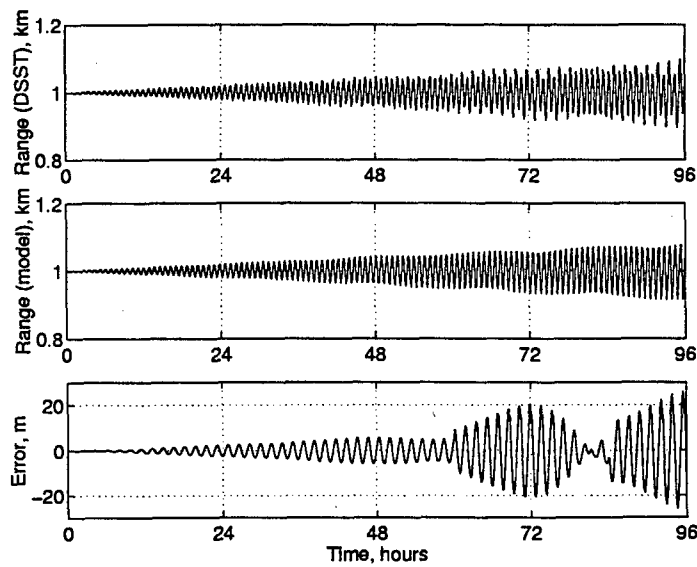


Figure 5: Comparison of the total separation ( $\rho$ ) of satellites 1 and 3 from DSST and  $J_2$  model for a 800 km, polar reference orbit. The satellites are in a 1 km circular formation.

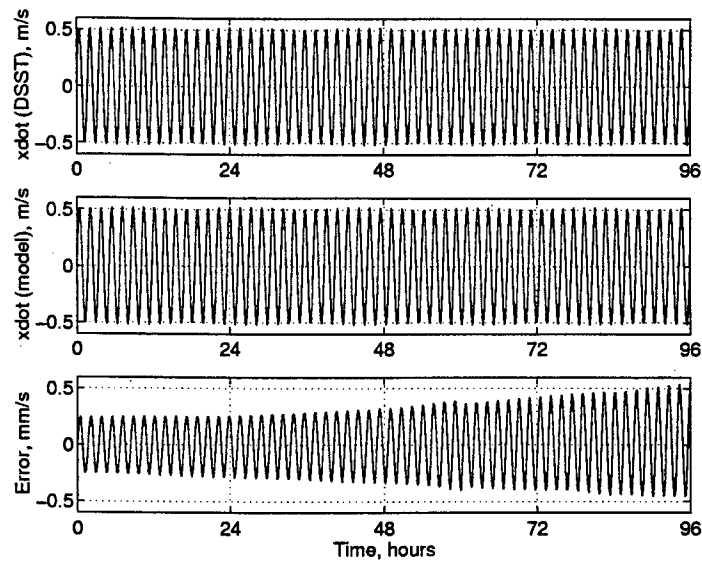


Figure 6: Comparison of the radial relative velocity ( $\dot{x}$ ) of satellites 1 and 3 from DSST and  $J_2$  model for a 800 km, polar reference orbit. The satellites are in a 1 km circular formation.

The maximum errors in the  $J_2$  model are only a few mm/s. The errors shown here are typical of all the cases.

Fig. 10 shows the results for the range rate between the satellites. The error in the  $J_2$  model is about 30 mm/s after four days. This error is primarily caused by the error in the  $y$  component. Once again, the error results are typical.

The equations in the  $J_2$  model predict that there will be no secular growth in the relative separation at critical inclination for satellites that have out-of-plane separation caused only by differences in  $\Omega$ . Figs. 11 through 13 show that the growth in relative separation, relative velocity, and range rate is small according to DSST.

## Satellites 1 and 2

Satellites 1 and 2 primarily attain out-of-plane motion through differences in inclination. Consequently, the differential effects of  $J_2$  are important. According to the  $J_2$  model the largest change in separation should occur near an inclination of  $45^\circ$  and be mostly in the along-track component. DSST runs showed this to be true. The separations are compared in Figs. 14 and 15. Fig. 14 shows the large secular growth in the along-track term which leads to a large change in the total separation. Fig. 16 shows the range rate comparison. This is the maximum growth in range rate for the 1 km circular formations.

Fig. 17 shows the cross-track component for satellites 1 and 2 for a polar reference orbit. The growth in the component is relatively small, but this is the inclination at which the maximum cross-track growth occurs. Fig. 18 shows the relative velocity. This is the maximum relative velocity for the 1 km circular formations.

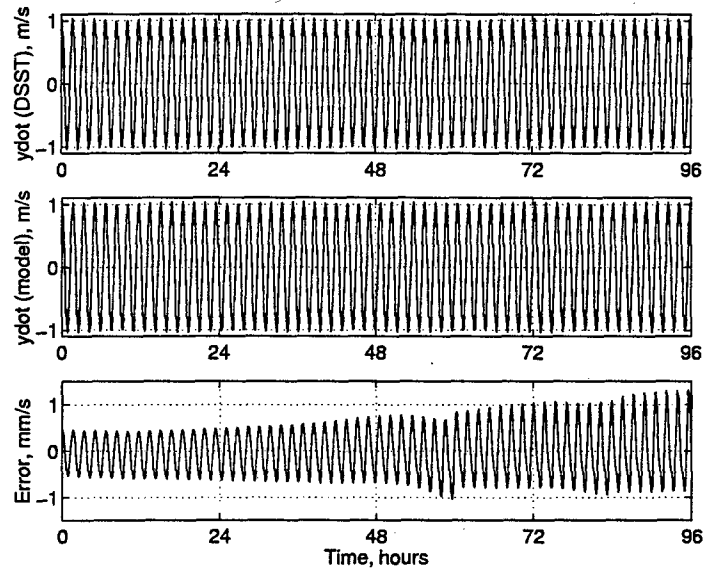


Figure 7: Comparison of the along-track relative velocity ( $\dot{y}$ ) of satellites 1 and 3 from DSST and  $J_2$  model for a 800 km polar reference orbit. The satellites are in a 1 km circular formation.

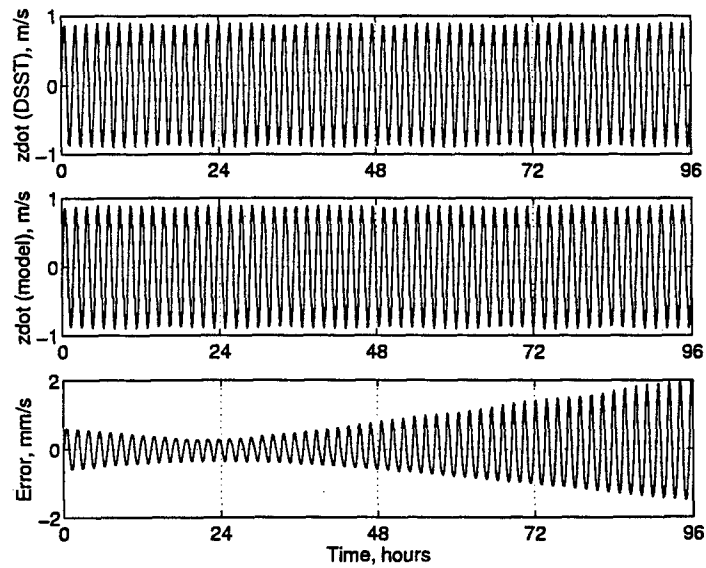


Figure 8: Comparison of the cross-track relative velocity ( $\dot{z}$ ) of satellites 1 and 3 from DSST and  $J_2$  model for a 800 km, polar reference orbit. The satellites are in a 1 km circular formation.

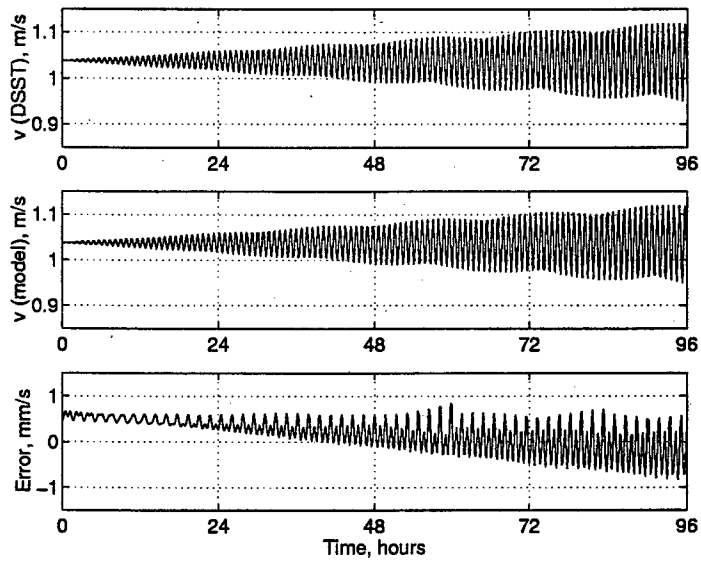


Figure 9: Comparison of the relative velocity ( $v$ ) of satellites 1 and 3 from DSST and  $J_2$  model for a 800 km polar reference orbit. The satellites are in a 1 km circular formation.

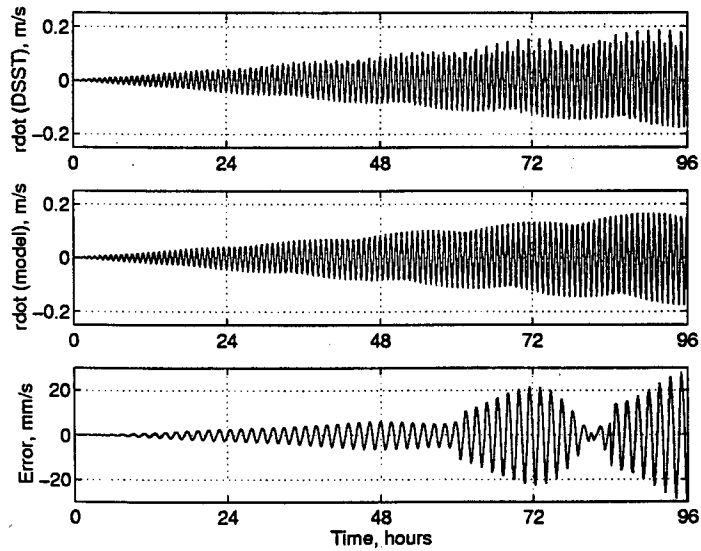


Figure 10: Comparison of the range rate ( $\dot{\rho}$ ) of satellites 1 and 3 from DSST and  $J_2$  model for a 800 km, polar reference orbit. The satellites are in a 1 km circular formation.

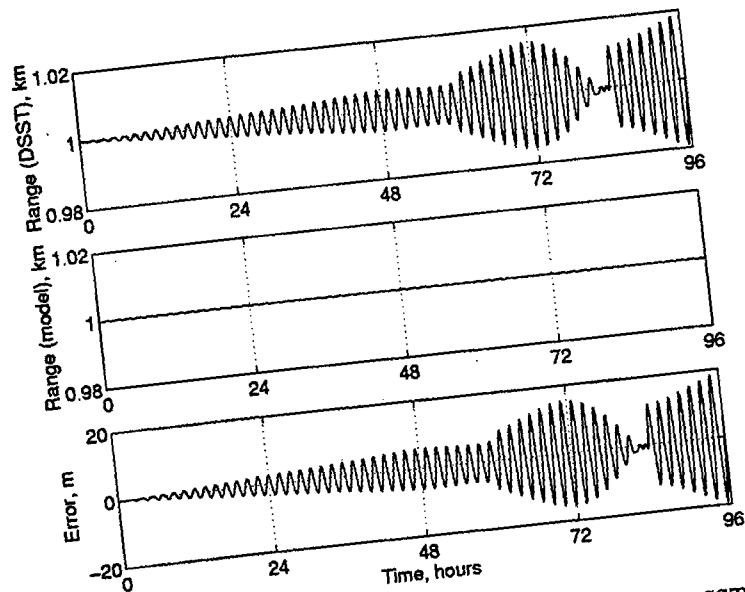


Figure 11: Comparison of the total separation ( $\rho$ ) of satellites 1 and 3 from DSST and  $J_2$  model for a 800 km, critically inclined reference orbit. The satellites are in a 1 km circular formation.

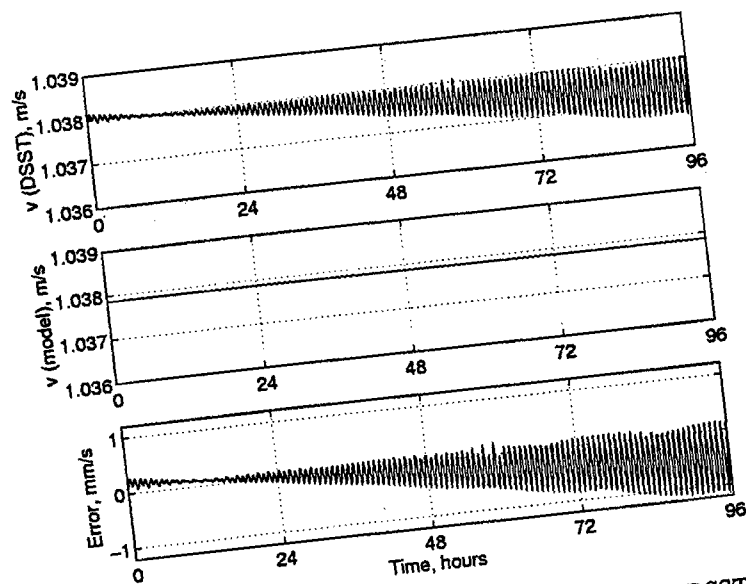


Figure 12: Comparison of the relative velocity ( $v$ ) of satellites 1 and 3 from DSST and  $J_2$  model for a 800 km, critically inclined reference orbit. The satellites are in a 1 km circular formation.

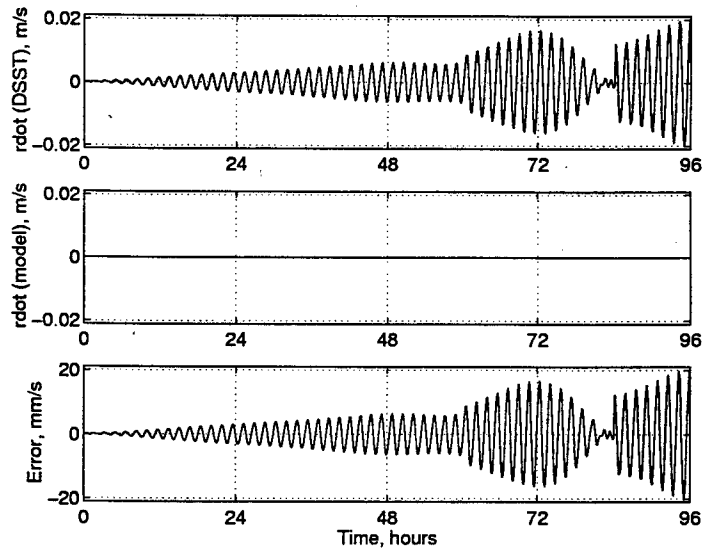


Figure 13: Comparison of the range rate ( $\dot{\rho}$ ) of satellites 1 and 3 from DSST and  $J_2$  model for a 800 km, critically inclined reference orbit. The satellites are in a 1 km circular formation.

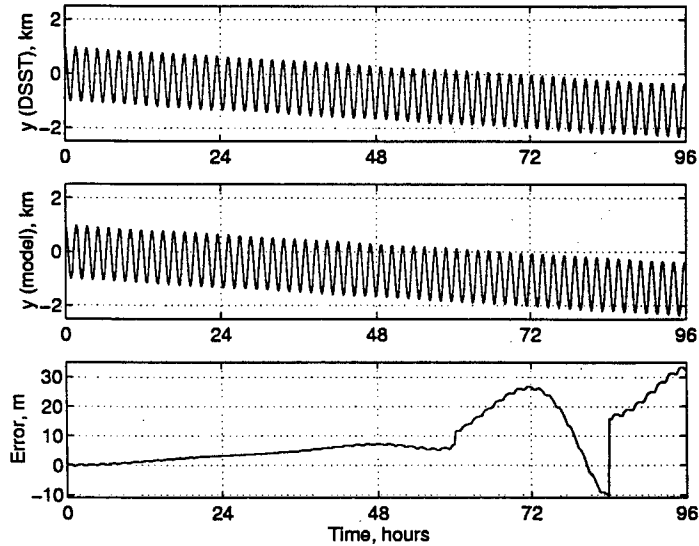


Figure 14: Comparison of the along-track separation ( $y$ ) of satellites 1 and 2 from DSST and  $J_2$  model for a 800 km, 45° inclination reference orbit. The satellites are in a 1 km circular formation.

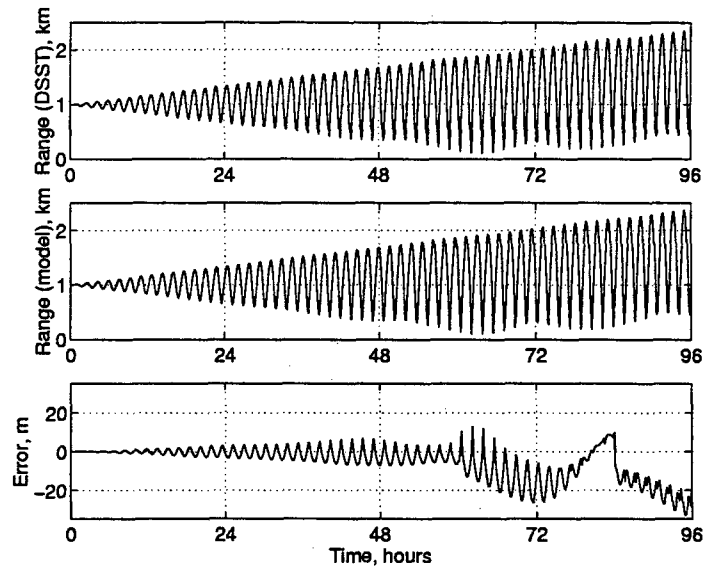


Figure 15: Comparison of the total separation ( $\rho$ ) of satellites 1 and 2 from DSST and  $J_2$  model for a 800 km,  $45^\circ$  inclination reference orbit. The satellites are in a 1 km circular formation.

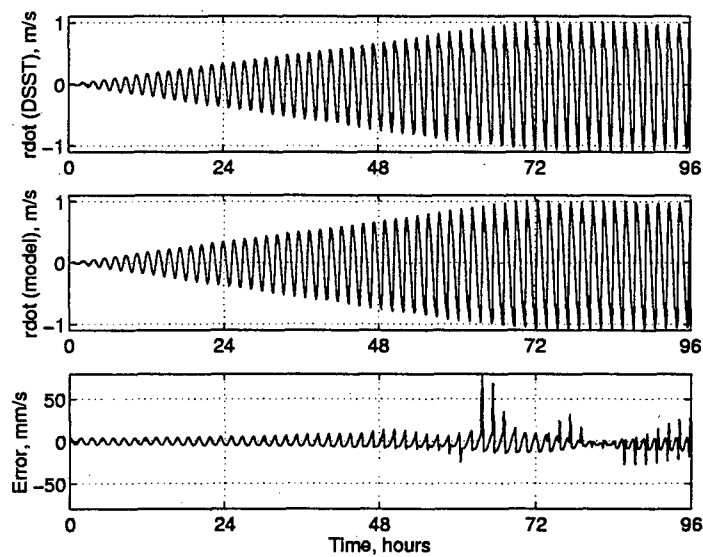


Figure 16: Comparison of the range rate ( $\dot{\rho}$ ) between satellites 1 and 2 from DSST and  $J_2$  model for a 800 km,  $45^\circ$  inclination reference orbit. The satellites are in a 1 km circular formation.

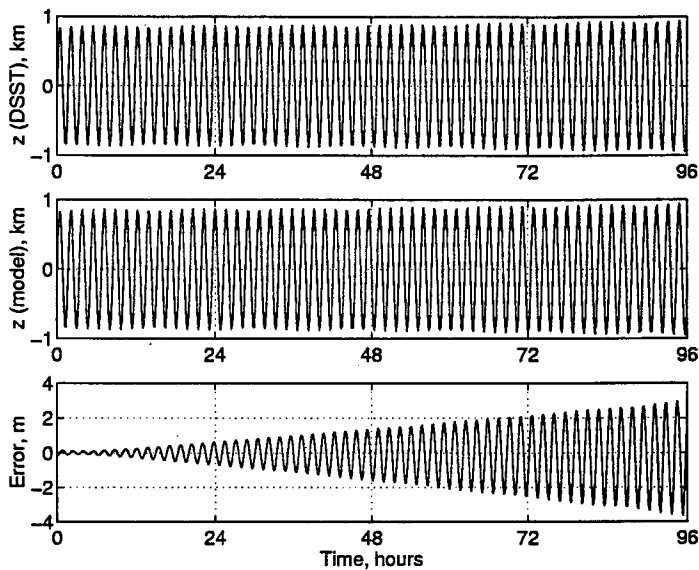


Figure 17: Comparison of the cross-track separation ( $z$ ) between satellites 1 and 2 from DSST and  $J_2$  model for a 800 km, polar reference orbit. The satellites are in a 1 km circular formation.

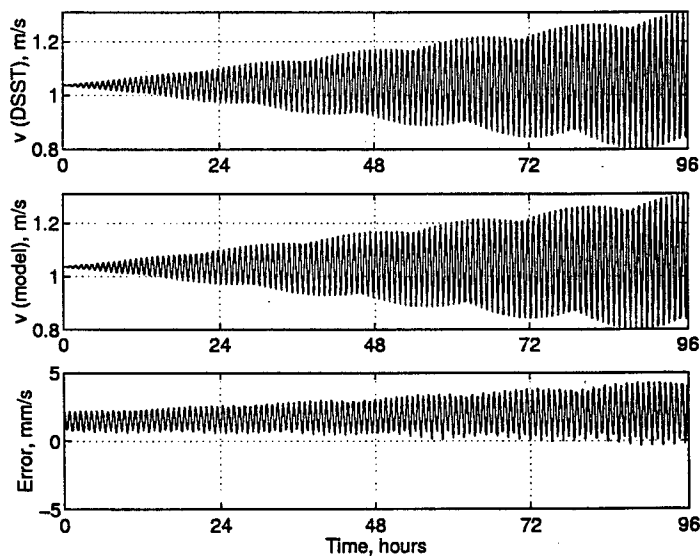


Figure 18: Comparison of the relative velocity ( $v$ ) between satellites 1 and 2 from DSST and  $J_2$  model for a 800 km, polar reference orbit. The satellites are in a 1 km circular formation.

## Summary

The largest contributor to the error in the  $J_2$  model compared to DSST was consistently the along-track position component. Running a case with  $J_2$  only showed that only a small portion of the error is unmodeled  $J_2$  effects. Most likely these are higher order  $J_2^2$  effects. Most of the along-track error is caused by unmodeled solar radiation pressure. This was shown by a case run without solar radiation pressure. The error was much lower for the case run with SRP turned off. The epoch is near the autumnal equinox and the orbit plane is nearly parallel to the sun-earth vector. This explains why the effect is mostly in the along-track direction. The effects of SRP need further investigation to assure that they are real. Regardless, the accuracy of the model should improve if  $\Omega$  is changed or an epoch not so close to equinox is used. A projected circular case was run at 600 km altitude. Unexpectedly, the relative position errors were slightly smaller at the lower altitude. However, this can be explained by the fact that SRP was the primary cause of the errors. Projected circular formations with radii of 100 m and 10 km were also examined. All the errors were much larger for the 10 km projected circular formation because the greater separations translate into greater differential perturbations. However, the 100 m projected circular formation still had errors as large as the 1 km projected circular formations. In general, the  $J_2$  model was accurate over four days to within 1 m in the radial component, a few meters in cross-track, and less than 50 m in along-track and range. The accuracy in the velocity components was better than 10 mm/s. Finally, the range rate accuracy was less than 1 cm/s. The exception to these accuracy comparisons was the formation that had a 10 km nominal separation. The maximum errors in each component for the all the cases examined are given in the Appendix.

The extrema of the relative motion from DSST is also contained in a table in the Appendix. As expected the maximum perturbations were for the formation with the largest separation. The formations at an inclination of  $45^\circ$  had the largest changes in separation and range rate for the 1 km formations. In fact, the separation was as low as 50 m and as large as 2.56 km for the projected circular formation at  $45^\circ$  inclination. However, the polar orbits had the largest relative velocities.

## CONCLUSIONS

A model that over several days accurately describes the mean relative motion, relative velocity, and range rate of satellites flying in formation has been developed. The model includes the absolute and differential effects of  $J_2$  on the dynamics. The absolute effects of  $J_2$  cause the in-plane and out-of-plane motion to have different frequencies. This causes a long periodic variation in the separation between the satellites. For satellites without inclination differences this is the primary effect. Differential  $J_2$  effects occur for satellites with inclination differences. These cause the separation between the satellites to grow secularly. The model has been tested by comparing the results from mean element propagations performed using the Draper Semianalytic Satellite Theory for a number of inclinations, altitudes, formation types, and formation sizes. The primary error source not modeled was solar radiation pressure which caused an unmodeled along-track drift. The model provides a great improvement over using the unperturbed Hill's equations and provides physical insight into the errors in using Hill's equations.

In addition, the relative motion, relative velocity, and range rate expected between satellites flying in formation has been quantified for a number of formations. This information will be important for the design of relative motion sensors such as intersatellite range and range rate devices. This will provide for better relative motion and velocity estimation which is a critical technology for flying satellites in close formations.

There are several areas of future work related to this effort. The bias in the initial conditions of the  $J_2$  model needs to be reflected in the initial conditions used in DSST. Also, the unusual SRP effects need further investigation to see if the effects are real.  $J_2^2$ ,  $J_3$ , and  $J_4$  perturbations on  $\Omega$ ,  $i$ , and  $M$  can be added into the equations. Finally, the equations developed here are valid for low eccentricity. Expanding the equations to highly eccentric orbits needs investigation.

## References

- [1] Kyle T. Alfriend, Hanspeter Schaub, and Dong-Woo Gim. Gravitational perturbations, nonlinearity and circular orbit assumption effects on formation flying control strategies. In *Proceedings of the AAS GNC Conference*, Breckenridge, CO, January 2000. AAS 00-012.
- [2] D. A. Danielson. Semianalytic satellite theory. Technical Report NPS-MA-95-002, Naval Postgraduate School, 1994.
- [3] Martin E. Feiger. An Evaluation of Semianalytic Satellite Theory Against Long Arcs of Real Data for Highly Eccentric Orbits. Master's thesis, Massachusetts Institute of Technology, 1995.
- [4] Daniel J. Fonte. PC based orbit determination. In *Proceedings of the AIAA/AAS Astrodynamics Conference*, Scottsdale, AZ, August 1994. AIAA 94-3776.
- [5] Dong-Woo Gim and Kyle T. Alfriend. The state transition matrix of relative motion for the perturbed non-circular reference orbit. In *Proceedings of the AAS/AIAA Space Flight Mechanics Meeting*, Santa Barbara, CA, February 2001. AAS 01-222.
- [6] G. W. Hill. Researches in the lunar theory. *American Journal of Mathematics*, 1:5-26, 1878.
- [7] Jonathan P. How and Robert Michael Tillerson. Analysis of the impact of sensor noise on formation flying control. In *Proceedings of the AIAA Guidance, Navigation, and Control Conference*, Montreal, Quebec, August 2001. AIAA 2001-4092.
- [8] Gokhan Inalhan and Jonathan P. How. Relative dynamics and control of spacecraft formations in eccentric orbits. In *Proceedings of the AIAA Guidance, Navigation, and Control Conference*, Denver, CO, August 2000. AIAA 2000-4443.
- [9] D. F. Lawden. *Optimal Trajectories for Space Navigation*. Butterworths, London, 1963.
- [10] W. McClain. A recursively formulated first-order semianalytic artificial satellite theory based on the generalized method of averaging. Technical Report NAS 5-24300, June 1978. Task Assignment 880.
- [11] Ronald Proulx, Paul Cefola, and Kim Luu. The role of short-periodic motion in formation flying of satellites with large differential area to mass ratio. In *Proceedings of the AAS/AIAA Astrodynamics Specialists Conference*, Quebec City, Canada, August 2001. AAS 01-167.
- [12] Chris Sabol, Rich Burns, and Craig A. McLaughlin. Satellite formation flying design and evolution. *Journal of Spacecraft and Rockets*, 38(2):270-278, March-April 2001.
- [13] Chris Sabol, Paul Cefola, and Rich Metzinger. Application of sun-synchronous, critically inclined orbits to global personal communications systems. In *Proceedings of the AAS/AIAA Space Flight Mechanics Meeting*, Albuquerque, NM, February 1995. AAS 95-222.
- [14] Kenneth H. Schatten, Philip H. Scherrer, Leif Svalgaard, and John M. Wilcox. Using dynamo theory to predict the sunspot number during solar cycle 21. *Geophysical Research Letters*, 5(5):411-414, May 1978.

- [15] Sabatino Sofia, Peter Fox, and Kenneth Schatten. Forecast update for activity cycle 23 from a dynamo-based method. *Geophysical Research Letters*, 25(22):4149–4152, November 1998.
- [16] David A. Vallado. *Fundamentals of Astrodynamics and Applications*. Space Technology Series. McGraw-Hill, New York, 1997.

Table 5: Maximum errors in  $J_2$  model relative motion compared to DSST

Error in:	$x$	$y$	$z$	$\rho$	$\dot{x}$	$\dot{y}$	$\dot{z}$	$v$	$\dot{\rho}$
	[m]	[m]	[m]	[m]	[mm/s]	[mm/s]	[mm/s]	[mm/s]	[mm/s]
<b>Formation</b>									
<u>Circ.</u>									
$i = 1^\circ$									
Sats1-2	0.42	34.14	8.04	31.69	0.72	1.78	8.96	6.96	63.09
Sats1-3	0.64	45.31	8.18	43.15	0.87	1.90	8.33	5.33	58.55
$i = 28.5^\circ$									
Sats1-2	0.58	35.14	1.60	33.91	1.07	5.50	2.15	4.61	45.87
Sats1-3	0.41	51.12	3.43	48.18	0.55	1.36	3.54	2.82	72.76
$J_2$ Only									
Sats1-2	0.31	5.48	1.88	5.33	0.50	4.35	2.15	4.23	5.35
Sats1-3	0.62	12.55	2.51	11.22	0.76	1.49	2.90	2.65	18.93
No SRP									
Sats1-2	0.61	8.26	1.57	6.74	1.06	5.45	2.15	4.28	7.60
Sats1-3	0.45	10.05	3.43	9.57	0.53	1.08	3.53	2.79	16.12
$i = 45^\circ$									
Sats1-2	0.50	33.43	2.35	33.12	0.67	5.21	1.89	4.95	79.15
Sats1-3	0.34	41.59	1.60	40.44	0.28	0.87	1.78	1.63	48.09
$i = 63.435^\circ$									
Sats1-2	0.90	20.02	1.71	18.83	0.93	4.99	3.03	4.17	21.61
Sats1-3	0.34	20.11	1.67	19.25	0.22	0.52	1.50	1.15	20.31
$i = 90^\circ$									
Sats1-2	0.44	26.31	3.67	25.46	0.68	1.00	5.25	4.30	36.56
Sats1-3	0.58	27.10	2.50	26.02	0.54	1.31	1.98	0.84	30.32
<u>Proj. Circ.</u>									
$i = 1^\circ$									
Sats1-2	0.39	33.97	9.30	31.28	0.72	1.75	10.36	8.32	61.15
Sats1-3	0.63	47.50	9.47	45.10	0.83	1.85	9.64	6.60	67.39
$i = 28.5^\circ$									
Sats1-2	0.62	33.74	1.85	32.55	1.10	6.05	2.48	5.10	48.76
Sats1-3	0.48	52.90	4.00	49.92	0.54	1.28	4.12	3.39	74.37
Alt=600km									
Sats1-2	1.54	30.64	3.45	27.53	2.33	8.27	3.96	5.27	33.62
Sats1-3	1.32	46.08	6.40	41.82	0.99	2.63	6.83	4.84	65.55
$\rho_0=10$ km									
Sats1-2	71.19	135.29	15.07	106.51	33.41	94.34	28.41	60.46	190.16
Sats1-3	17.74	169.90	40.21	159.27	10.09	14.07	39.49	29.02	243.81
$\rho_0=100$ m									
Sats1-2	0.44	40.41	0.22	39.07	0.23	1.22	0.25	0.84	51.53
Sats1-3	0.39	42.21	0.42	40.42	0.20	0.77	0.45	0.76	58.71
$i = 45^\circ$									
Sats1-2	0.61	33.10	2.74	32.82	0.71	5.85	2.21	5.56	82.92
Sats1-3	0.31	42.71	1.84	41.37	0.27	0.81	2.04	1.88	44.95
$i = 63.435^\circ$									
Sats1-2	1.00	20.44	1.98	19.17	1.01	5.69	3.50	4.70	32.14
Sats1-3	0.33	21.01	1.93	19.97	0.25	0.51	1.73	1.39	19.13
$i = 90^\circ$									
Sats1-2	0.43	26.31	4.26	25.42	0.65	1.05	6.08	5.17	38.63
Sats1-3	0.58	27.26	2.89	26.12	0.54	1.33	2.29	1.07	28.38

Table 6: Extrema from DSST for different formations

Extrema in:	$\rho_{min}$ [km]	$\rho_{max}$ [km]	$v$ [m/s]	$\dot{\rho}$ [m/s]
Formation:				
<u>Circ.</u>				
<u><math>i = 1^\circ</math></u>				
Sats1-2	0.64	1.27	1.30	0.64
Sats1-3	0.63	1.29	1.30	0.66
<u><math>i = 28.5^\circ</math></u>				
Sats1-2	0.19	2.18	1.22	1.13
Sats1-3	0.72	1.22	1.25	0.52
<u><math>i = 45^\circ</math></u>				
Sats1-2	0.11	2.35	1.09	1.08
Sats1-3	0.84	1.15	1.16	0.27
<u><math>i = 63.435^\circ</math></u>				
Sats1-2	0.14	2.12	1.18	1.13
Sats1-3	0.98	1.02	1.04	0.02
<u><math>i = 90^\circ</math></u>				
Sats1-2	0.74	1.25	1.31	0.54
Sats1-3	0.89	1.10	1.12	0.19
<u>Proj. Circ.</u>				
<u><math>i = 1^\circ</math></u>				
Sats1-2	0.66	1.36	1.39	0.71
Sats1-3	0.63	1.37	1.40	0.76
<u><math>i = 28.5^\circ</math></u>				
Sats1-2	0.20	2.38	1.32	1.22
Sats1-3	0.76	1.32	1.33	0.56
Alt=600km				
Sats1-2	0.17	2.60	1.38	1.29
Sats1-3	0.72	1.33	1.41	0.65
$\rho'_0=10$ km				
Sats1-2	2.15	24.19	13.18	12.25
Sats1-3	7.77	12.95	13.29	5.33
$\rho'_0=100$ m				
Sats1-2	0.02	0.23	0.13	0.12
Sats1-3	0.05	0.16	0.13	0.09
<u><math>i = 45^\circ</math></u>				
Sats1-2	0.05	2.56	2.56	1.16
Sats1-3	0.87	1.21	1.25	0.35
<u><math>i = 63.435^\circ</math></u>				
Sats1-2	0.14	2.29	1.29	1.25
Sats1-3	0.99	1.12	1.16	0.13
<u><math>i = 90^\circ</math></u>				
Sats1-2	0.78	1.36	1.41	0.61
Sats1-3	0.93	1.17	1.21	0.25